

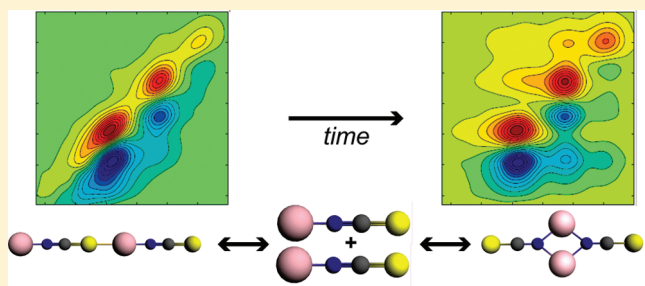
# Interdependence of Conformational and Chemical Reaction Dynamics during Ion Assembly in Polar Solvents

Minbiao Ji,<sup>†,‡,||</sup> Robert W. Hartsock,<sup>†,§</sup> Zheng Sun,<sup>†</sup> and Kelly J. Gaffney\*,<sup>†</sup>

<sup>†</sup>PULSE Institute, SLAC National Accelerator Laboratory, <sup>‡</sup>Department of Physics, and <sup>§</sup>Department of Chemistry, Stanford University, Stanford, California 94305, United States

 Supporting Information

**ABSTRACT:** We have utilized time-resolved vibrational spectroscopy to study the interdependence of the conformational and chemical reaction dynamics of ion assembly in solution. We investigated the chemical interconversion dynamics of the LiNCS ion pair and the  $(\text{LiNCS})_2$  ion-pair dimer, as well as the spectral diffusion dynamics of these ionic assemblies. For the strongly coordinating Lewis base solvents benzonitrile, dimethyl carbonate, and ethyl acetate, we observe  $\text{Li}^+$  coordination by both solvent molecules and NCS<sup>-</sup> anions, while the weak Lewis base solvent nitromethane shows no evidence for solvent coordination of  $\text{Li}^+$  ions. The strong interaction between the ion-pair dimer structure and the Lewis base solvents leads to ion-pair dimer solvation dynamics that proceed more slowly than the ion-pair dimer dissociation. We have attributed the slow spectral diffusion dynamics to electrostatic reorganization of the solvent molecules coordinated to the  $\text{Li}^+$  cations present in the ion-pair dimer structure and concluded that the dissociation of ion-pair dimers depends more critically on longer length scale electrostatic reorganization. This unusual inversion of the conformational and chemical reaction rates does not occur for ion-pair dimer dissociation in nitromethane or for ion pair association in any of the solvents.



## I. INTRODUCTION

Transition state theory represents the most widely applied theory for describing chemical reaction rates. The accuracy of transition state theory depends upon the relative rate of conformational equilibration of the reactant and product species and the rate of chemical exchange between the reactant and product structures.<sup>1–3</sup> Transition state theory uses a thermally weighted density of states to approximate the probability of reaching the transition state that separates reactants from products. For this Boltzmann factor to accurately reflect the probability of reaching the transition state, the reactant conformational phase space must be fully sampled prior to chemical reaction.

The potentially significant interdependence of conformational and chemical dynamics has been most widely and contentiously investigated in enzymatic systems.<sup>4–9</sup> The correlation between the conformational dynamics measured with NMR<sup>4</sup> and the catalytic reaction rates of enzymes and the nonstationary catalytic reaction rate of single enzyme molecules<sup>8,9</sup> has been interpreted to indicate that conformational motions can trigger catalytic reactions. These interpretations, however, have been disputed by others arguing that these measurements do not necessitate the inclusion of dynamical effects to transition state theory to accurately describe enzymatic catalysis.<sup>10,11</sup>

The fundamental importance of the interplay between conformational and chemical dynamics in biochemical systems has inspired our investigation of chemical and conformational dynamics in a comparatively simple chemical reaction, the assembly

of lithium and thiocyanate ions in aprotic solvents. The equilibrium structure of these ions depends critically on the solvent and ionic concentration, with the ionic configurations varying from dissociated ions to contact ion pairs, ion-pair dimers, and ion-pair tetramers.<sup>12–15</sup> Chabanel has shown that the equilibrium configuration depends on the dielectric and electron donor properties of the solvent,<sup>16</sup> indicating that both long-range and short-range ion–solvent interactions influence the thermodynamics of ion assembly.

The dynamics of ion assembly and solvation also have a wide-ranging impact in chemistry, biology, and materials science.<sup>17–22</sup> Ion solvation and assembly influence mobility, polyelectrolyte structure, and crystal nucleation. Understanding the physicochemical properties of ionic solutions that determine the mobility of lithium cations in aprotic solvents has particular technological significance due to the importance of lithium salt electrolytes in secondary lithium ion batteries.<sup>23</sup> Understanding the dynamics of these aggregates, as well as the dynamics of their formation and dissociation, will help us understand how solute–solvent interactions control the properties of electrolytes.

We have chosen to use time-resolved vibrational spectroscopy to investigate the conformational and chemical dynamics of ion assemblies. Vibrational spectroscopy has proven to be a powerful

**Received:** June 16, 2011

**Revised:** August 17, 2011

**Published:** August 19, 2011

method for identifying and distinguishing the various ionic structures in solution<sup>24–29</sup> with many studies utilizing the CN stretch of the thiocyanate ion to determine the ionic configuration.<sup>30,31</sup> The CN stretch has a long vibrational excited state lifetime, making it a good chromophore for time-resolved studies.<sup>32–37</sup> The sensitivity of vibrational spectroscopy to the thiocyanate ionic configuration makes the dynamics of ion assembly amenable to two-dimensional infrared (2DIR) spectroscopy studies. We demonstrated the feasibility of the measurements in a prior study,<sup>30</sup> where we characterized the dynamics of LiNCS ion-pair dimer formation and dissociation in benzonitrile solution. The present study assesses the solvent dependence of these exchange dynamics and characterizes the spectral diffusion dynamics of each ionic configuration. We attribute the spectral heterogeneity to the vibrational Stark effect<sup>38,39</sup> and the spectral diffusion dynamics to electric field fluctuations and propose that the slowest spectral diffusion dynamics result from reorganization of the solvent molecules coordinated to the lithium ions in the ionic assemblies. This conclusion correlates with the strong solvent dependence of the spectral diffusion dynamics, with strongly coordinating solvents like benzonitrile, dimethyl carbonate, and ethyl acetate having distinctly slower dynamics than the weakly coordinating nitromethane. We emphasize the experimental results observed for nitromethane and benzonitrile solutions to highlight the important distinctions between weakly and strongly coordinating solvents.

By independently assessing the conformational dynamics of each structurally distinct ionic configuration, as well as the chemical exchange dynamics between these distinct configurations, we have been able to investigate the interdependence of the conformational and chemical dynamics and find that the interplay depends critically on the chemical properties of the solvent.

## II. EXPERIMENTAL AND THEORETICAL METHODS

The laser system employed in the experiments was built based on a design that has been described in detail elsewhere.<sup>40</sup> We generate 800 nm pulses with a Ti:Sapphire oscillator (KM Laboratories) and regenerative amplifier (Spitfire, Spectra-Physics) laser system at 1 kHz. The 800 nm pulses with 45 fs duration and ~1 mJ per pulse were used to pump an optical parametric amplifier (OPA800CF, Spectra-Physics) to produce near-IR pulses at ~1.4 and ~1.9  $\mu\text{m}$  which were utilized to generate mid-IR pulses at  $2050 \text{ cm}^{-1}$  in a 0.5 mm thick AgGaS<sub>2</sub> crystal by difference frequency generation. The power spectrum of the mid-IR pulses had a Gaussian envelope with a  $\sim 250 \text{ cm}^{-1}$  bandwidth (full width at half-maximum). After generation, the mid-IR pulses propagate through an experimental setup purged with dry and CO<sub>2</sub> scrubbed air. We measured the pulse chirp with frequency-resolved optical gating measurements in a transient grating geometry.<sup>40</sup> We used CaF<sub>2</sub> plates with different thicknesses to compensate for the linear dispersion introduced by other dielectric materials in the setup, particularly a Ge Brewster plate. This setup produced transform-limited mid-IR pulses with a pulse duration of  $\sim 65$  fs at the sample.

The experimental details and principles of multidimensional vibrational correlation spectroscopy, generally termed two-dimensional infrared (2DIR) spectroscopy, have been described in detail elsewhere.<sup>40,41</sup> We focus three mid-IR pulses with an off-axis parabolic mirror (focal length of 150 cm) onto the sample in a noncollinear geometry and collimate the beams after the

sample with another off-axis parabolic mirror (focal length of 150 cm). The spot size of the IR beams at the sample position is approximately 50  $\mu\text{m}$  in diameter. We control the relative time of these three pulses with computer controlled translational stages (ANT-50 L, Aerotech). The sample emits the signal in a unique phase-matched direction, which we overlap with a local oscillator pulse for heterodyne detection. A grating in a spectrometer (iHR320, Horiba) disperses the heterodyned signal onto the top stripe of a dual 32  $\times$  2 element mercury–cadmium–telluride (MCT) array detector with high speed data acquisition electronics (FPAS-6416-D, Infrared Systems Development Corp.). For polarization resolved pump–probe measurements, the mid-IR pulses are split into the pump and probe beams with a relative intensity of 9:1 and focused onto the sample. The probe beam is collimated after the sample and is dispersed through a spectrometer onto the same MCT array detector used in the 2DIR experiments. We use wire grid polarizers to control the polarization of the pump and probe pulses. We placed them in the pump and probe beam before the sample and in front of the spectrometer.

We utilized Amsterdam Density Function (ADF) to calculate gas-phase structures and vibrational absorption spectra for a variety of LiNCS ionic structures.<sup>42,43</sup> We utilized the VWN local density functional in conjunction with the triple- $\zeta$  polarized (TZP) basis set without any frozen cores when optimizing the geometry of the dimer structures. The same settings were used when calculating the infrared absorption spectra analytically. Scalar relativistic effects were left on during the calculations. All structure geometries were preoptimized using the molecular mechanics approach.

The detailed preparation procedure for LiNCS ion pair and dimer equilibrium solutions has been described elsewhere.<sup>30,44</sup> We purchased benzonitrile (BN), nitromethane (MeNO<sub>2</sub>), dimethyl carbonate (DMC), ethyl acetate (EtAct), and LiNCS hydrate from Sigma-Aldrich. We used the solvents as received and dried the LiSCN $\cdot$ xH<sub>2</sub>O with a literature procedure.<sup>44</sup> We prepared the solutions by dissolving LiNCS in each solvent and then centrifuging the solutions for 15 min to precipitate the suspended particles. We sealed the sample between two CaF<sub>2</sub> windows spaced by a 3  $\mu\text{m}$  PET spacer to generate a maximum absorbance of roughly 0.4 for the 1.2 M LiNCS solutions. We performed the vibrational measurements at 22 °C over a spectral range from 1984 to 2110  $\text{cm}^{-1}$  with a resolution of 4  $\text{cm}^{-1}$ .

## III. RESULTS

**III.A. Vibrational Spectroscopy.** Figure 1 shows the FTIR spectra in the spectral region of the CN stretch of NCS<sup>−</sup> for a 1.2 M LiNCS solution in BN and MeNO<sub>2</sub>. The peak at 2073  $\text{cm}^{-1}$  corresponds to the CN stretch absorption of the ion pair, the peak at 2042  $\text{cm}^{-1}$  to the CN stretch absorption of an ion-pair dimer with a quadrupole charge distribution (Q-dimer),<sup>15,45</sup> and the small blue-shifted peak in MeNO<sub>2</sub> at 2102  $\text{cm}^{-1}$  to the thiocyanate anion coordinating Li<sup>+</sup> cations with both the sulfur and nitrogen in a linear ion-pair dimer (L-dimer).<sup>14</sup> The thiocyanate anion in the linear ion-pair dimer that only coordinates one Li<sup>+</sup> with nitrogen has a CN stretch absorption indistinguishable from the ion pair. While these assignments conform to the standard assignments in the literature, we have also performed a series of quantum chemical calculations that validate the assignments.

We used the VWN local density functional to optimize the geometry of the ion pair and the Q-dimer and L-dimer structures.

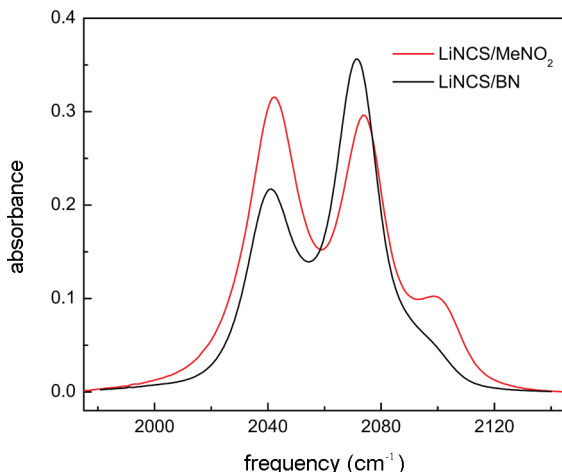


**Figure 1.** FTIR spectra of 1.2 M LiNCS in benzonitrile (BN) and nitromethane ( $\text{MeNO}_2$ ). The peak at  $\sim 2040 \text{ cm}^{-1}$  corresponds to an ion-pair dimer structure with a quadrupole charge distribution (Q-dimer); the peak at  $\sim 2070 \text{ cm}^{-1}$  corresponds to the LiNCS ion pair; and the peak at  $\sim 2100 \text{ cm}^{-1}$  corresponds to the  $\text{NCS}^-$  in a linear ion-pair dimer (L-dimer) that is coordinating two  $\text{Li}^+$  cations, one with the N atom and the other with the S atom.

The Q-dimer structure appears to be the lowest-energy dimer structure in the gas phase. Using a linear symmetry constraint, we calculated the structure and vibrational spectrum of the L-dimer, but relaxation of the symmetry constraint leads to spontaneous formation of the quadrupolar dimer structure. The lithium thiocyanate ion pair has a CN-stretch frequency of  $2071 \text{ cm}^{-1}$ . The Q-dimer contained two modes of vibration dominated by CN stretching, a symmetric ( $2045 \text{ cm}^{-1}$ ) Raman active vibration and an antisymmetric ( $2018 \text{ cm}^{-1}$ ) IR active vibration. The two CN-stretch vibrations of the L-dimer happen to be strongly localized to individual CN moieties. These vibrations occur at  $2077 \text{ cm}^{-1}$  for the thiocyanate nitrogen coordinating one  $\text{Li}^+$  and  $2126 \text{ cm}^{-1}$  for the thiocyanate that nitrogen and sulfur coordinate two  $\text{Li}^+$ . These calculation results parallel the findings of prior theoretical studies using ab initio<sup>46</sup> and semiempirical methods.<sup>47</sup> The different ionic structures appear in Figure 2, and the calculated and experimental CN stretch frequencies appear in Table 1.

The mid-IR spectroscopy of the dimer structures presents additional complications for the interpretation of chemical exchange and spectral diffusion dynamics because each dimer has two CN-stretch transitions. In the case of the Q-dimer structure, the presence of a center of inversion makes the asymmetric stretch of the two CN bonds IR active and the symmetric stretch Raman active. For the L-dimer, the two localized CN-stretches will both be IR active and generate two CN-stretch absorptions in the mid-IR absorption spectrum. For solutions possessing ion pairs, Q-dimers, and L-dimers, quantum chemical calculations predict four CN-stretch absorption peaks, but we only observe three distinct peaks experimentally. The theoretical calculations indicate that one of the L-dimer absorptions will overlap with the CN-stretch of the ion pair, though the roughly  $20 \text{ cm}^{-1}$  accuracy of the calculated frequencies leaves uncertainty about the spectral positions of the various ionic structures. This means that for the  $\text{MeNO}_2$  solution the peak nominally associated with the ion pair structure could also have a contribution from one of the L-dimer CN-stretch absorptions. This should

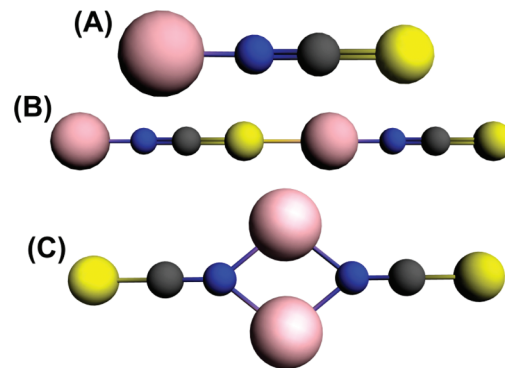


**Figure 2.** Calculated gas-phase structures for the (A) ion pair, (B) linear ion-pair dimer (L-dimer) structure, and (C) ion-pair dimer with a quadrupole charge distribution (Q-dimer). The figures used the following atomic color scheme: Li, mauve; N, blue; C, black; and S, yellow.

**Table 1. Experimental and Calculated Absorption Peak Frequency of LiNCS Ion Pair, Quadrupole Ion-Pair Dimer (Q-Dimer), and Linear Ion-Pair Dimer (L-Dimer) in  $\text{MeNO}_2$**

	exptl freq. ( $\text{cm}^{-1}$ )	calcd freq. ( $\text{cm}^{-1}$ )
pair	2073.6	2071
Q-dimer	2041.6	2018
L-dimer	2099	2126

have a minimal effect on the dynamics observed in BN, DMC, and EtAct solutions because of the very small L-dimer concentration.

The nature of the solute–solvent interaction also has a significant impact on the energetics and dynamics of ion assembly. As can be seen in Figure 3(A), complex formation between BN and  $\text{Li}^+$  leads to a significant shift in the CN stretch of BN. As can be seen in Figure 3(B), the asymmetric stretch of the nitro group of  $\text{MeNO}_2$  shows no evidence of complex formation with  $\text{Li}^+$ , strongly indicating that the nitro group at most forms a weak complex with the lithium cation. As will be addressed further in Section IV, these variations in the ion–solvent interaction result primarily from variations in the electron-donating properties of the solvent.

**III.B. 2DIR Spectroscopy Measurements of Chemical Exchange.** 2DIR spectroscopy monitors thermal equilibrium dynamics occurring on the picosecond time scale by vibrationally labeling molecules with their initial frequencies ( $\omega_\tau$ ) and then recording the final frequencies ( $\omega_m$ ) of the initially labeled molecules after an experimentally controlled waiting time ( $T_W$ ).<sup>48–50</sup> This spectroscopic technique can observe chemical exchange events as slow as a few times the vibrational lifetime and as fast as  $1/\Delta\omega$ , where  $\Delta\omega$  equals the vibrational frequency difference between the interconverting species. 2DIR spectra,  $S(\omega_\tau, \omega_m, T_W)$ , correlate the initial frequency ( $\omega_\tau$ ) and final frequency ( $\omega_m$ ) as a function of waiting time ( $T_W$ ). Figure 4(A) shows experimental 2DIR spectra for the LiNCS Q-dimer, ion pair system in BN at different  $T_W$ , while Figure 5(A) shows the analogous 2DIR spectra for the LiNCS L-dimer, Q-dimer, and ion pair system in  $\text{MeNO}_2$ . As can be seen in Figure 1, the L-dimer peak also occurs in BN, but the concentration is insufficient to robustly observe the rate of chemical exchange between the L-dimer and ion pair populations. The 2DIR spectra for the BN solution containing the spectral range associated with

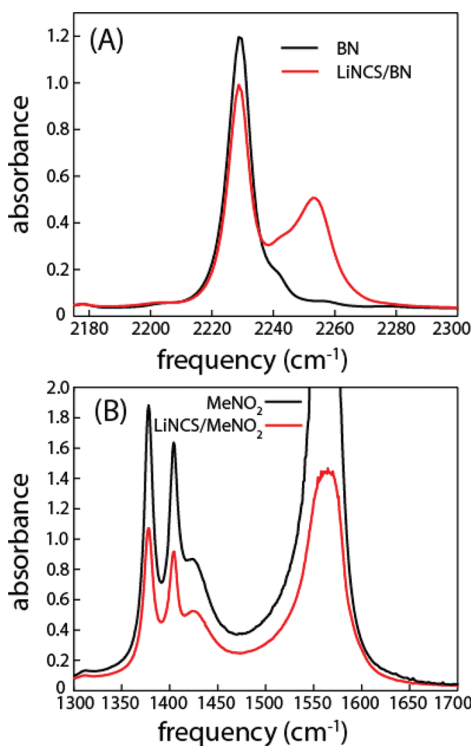


**Figure 3.** (A) FTIR spectra of benzonitrile (BN) and 1.2 M LiNCS in benzonitrile in the region of the CN stretch of BN. Note the appearance of a blue-shifted CN stretch due to direct coordination of  $\text{Li}^+$  cations by the cyano group on BN. (B) FTIR spectra of nitromethane ( $\text{MeNO}_2$ ) and 1.2 M LiNCS in nitromethane in the region of the symmetric and antisymmetric nitro-group stretching vibrations. We collected the pure solvent spectra with a  $2\ \mu\text{m}$  path length and the ionic solution spectra with a  $6\ \mu\text{m}$  path length.  $\text{MeNO}_2$  is a poor Lewis base, and we see no evidence for  $\text{Li}^+$  coordination by  $\text{MeNO}_2$ .

the L-dimer, as well as the 2DIR spectra for LiNCS in DMC and EtAct, can be found in the Supporting Information.

The spectra have multiple peaks representing various vibrational transitions. The red peaks along the diagonal ( $\omega_\tau = \omega_m$ ) correspond to the fundamental transitions ( $v = 0 \rightarrow 1$ ) for each distinct ionic configuration. The blue peaks, with  $\omega_m$  red-shifted from the diagonal peaks by the vibrational anharmonicity, correspond to the excited state transitions ( $v = 1 \rightarrow 2$ ) for the distinct ionic configurations.

The  $T_w$ -dependent spectra contain rich dynamical information about the solute–solvent interaction. Here we focus on the chemical dynamics of ion-pair dimer formation and dissociation that can be accessed by measuring the  $T_w$ -dependent cross-peak intensities of the 2DIR spectra. In the Discussion, we will use the peak positions shown in Figure 5(A) for LiNCS in  $\text{MeNO}_2$ , but the peak position variation between solvents is sufficiently small that the description also applies to the 2DIR spectra for the CN stretch of  $\text{NCS}^-$  dissolved in BN, DMC, and EtAct solutions. The peaks at  $(\omega_v, \omega_m)$  equal to  $(2074, 2074\ \text{cm}^{-1})$  and  $(2074, 2052\ \text{cm}^{-1})$  represent the  $v = 0 \rightarrow 1$  and  $v = 1 \rightarrow 2$  vibrational transitions of the LiNCS ion pair; the peaks at  $(2042, 2042\ \text{cm}^{-1})$  and  $(2042, 2022\ \text{cm}^{-1})$  represent the  $v = 0 \rightarrow 1$  and  $v = 1 \rightarrow 2$  vibrational transitions of the  $(\text{LiNCS})_2$  Q-dimer; and the peaks at  $(\omega_v, \omega_m)$  equal to  $(2099, 2099\ \text{cm}^{-1})$  and  $(2099, 2079\ \text{cm}^{-1})$  represent the  $v = 0 \rightarrow 1$  and  $v = 1 \rightarrow 2$  vibrational transitions of the  $(\text{LiNCS})_2$  L-dimer.

Twelve cross-peaks exist due to chemical exchange between the three distinct ionic structures, six of which can be clearly identified in Figure 5. The  $(\omega_v, \omega_m)$  cross-peak at  $(2042, 2074\ \text{cm}^{-1})$  results from the Q-dimer dissociating into two ion pairs. The cross-peak at  $(2042, 2099\ \text{cm}^{-1})$  results from the sequential transition from the Q-dimer to the L-dimer through an intermediate ion pair structure. The cross-peak at  $(2074, 2099\ \text{cm}^{-1})$  results from the association of two ion pairs to form an L-dimer. The cross-peak at  $(2074, 2022\ \text{cm}^{-1})$  results from

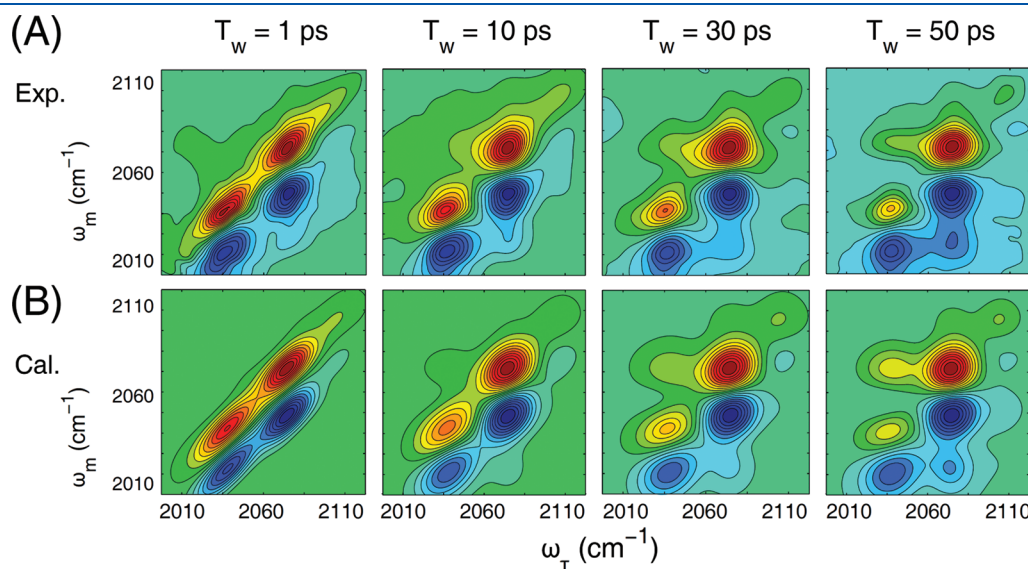


**Figure 4.** (A) Experimental  $T_w$ -dependent 2DIR spectra of the LiNCS ion-pair–Q-dimer equilibrium for 1.2 M LiNCS in benzonitrile (BN). The growth in cross-peak intensity as a function of  $T_w$  ( $\omega_v, \omega_m = 2042\ \text{cm}^{-1}, 2073\ \text{cm}^{-1}$ ) provides the clear signature of ion-pair–Q-dimer chemical exchange. Numerically calculated spectra appear in (B), with an exchange time constant of  $\tau_{\text{ex}} = 35 \pm 4\ \text{ps}$ . As can be seen in the 2DIR spectra for larger  $T_w$  time delays, a weak L-dimer signal becomes apparent in the 2DIR spectra for larger values of  $T_w$ , but the signal strength is insufficient to extract a robust exchange rate between the ion pair and L-dimer populations.

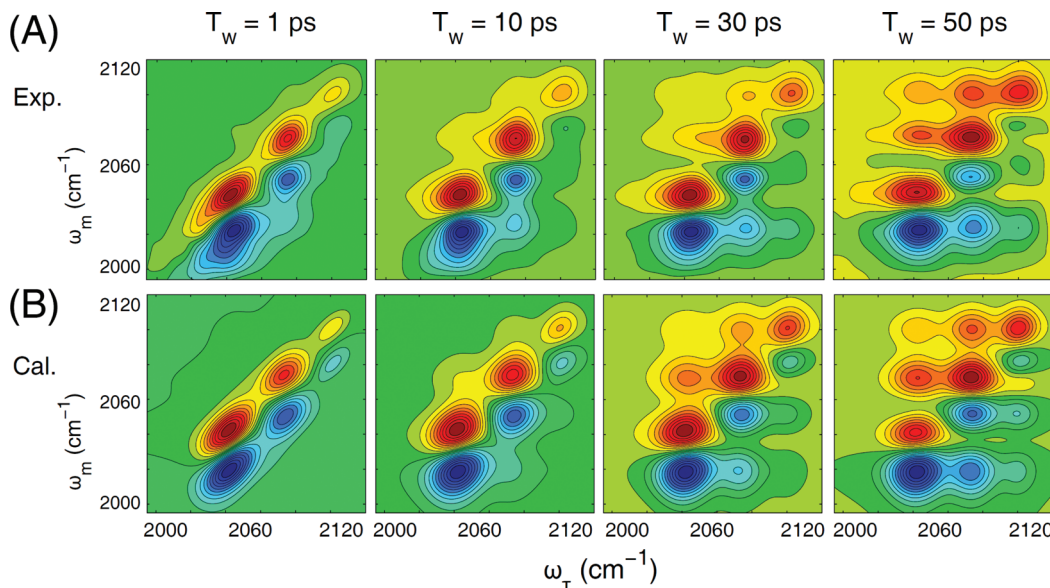


**Figure 5.** (A) Experimental  $T_W$ -dependent 2DIR spectra of the LiNCS ion pair–Q-dimer equilibrium for 1.2 M LiNCS in nitromethane ( $\text{MeNO}_2$ ). The growth in cross-peak intensity as a function of  $T_W$  ( $\omega_\tau, \omega_m = 2042 \text{ cm}^{-1}, 2074 \text{ cm}^{-1}$ ) provides the clear signature of ion pair–Q-dimer chemical exchange. Numerically calculated spectra appear in (B), with an exchange time constant of  $\tau_{\text{ex}} = 27 \pm 4 \text{ ps}$ .

the association of two ion pairs to form a Q-dimer, detected with the  $v = 1 \rightarrow 2$  transition of the Q-dimer. The cross-peak at ( $2099, 2052 \text{ cm}^{-1}$ ) results from the dissociation of the L-dimer into two ion pairs, detected with the  $v = 1 \rightarrow 2$  transition of the ion pair. The cross-peak at ( $2099, 2022 \text{ cm}^{-1}$ ) results from the sequential transition from the L-dimer to the Q-dimer through an intermediate ion pair structure, detected with the  $v = 1 \rightarrow 2$  transition of the Q-dimer. The six additional cross-peaks cannot be resolved because of overlap with the stronger  $v = 0 \rightarrow 1$  absorption of the ion pair and Q-dimer and the  $v = 1 \rightarrow 2$  absorption of the ion pair and L-dimer. The simulation shown in Figure 5(B) accounts for all 12 peaks that result from chemical exchange, as will be discussed in Section III.D.

As briefly mentioned in Section III.A, the presence of two CN-stretch absorption peaks for the L-dimer presents potential complications for the analysis of the 2DIR spectra. In particular, the coherent excitation of coupled oscillators can lead to multiple cross-peak signals and oscillations in pump probe measurements.<sup>51,52</sup> The coherent sources of cross-peak intensity will appear in the 2DIR spectrum for all values of  $T_W$ , providing a means of distinguishing these coherent signals from chemical exchange sources of cross-peak intensity. As can be seen for the  $T_W = 1 \text{ ps}$  spectra in Figure 5(A), we see no evidence for this source of off-diagonal signal. This appears to indicate that the two CN-stretch vibrations of the L-dimer do not couple strongly or that the missing CN-stretch absorption of the L-dimer has a much smaller absorption cross-section.

For  $T_W$  values, much larger than the excited state lifetime, the 2DIR spectra show a signal that results from vibrational relaxation induced heating of the solution.<sup>30</sup> We have limited our analysis to  $T_W \leq 60 \text{ ps}$  to ensure that this heating effect does not impact our data analysis. For a 60 ps waiting time, the cross-peak intensity exceeds the magnitude of the thermal contribution by a factor of 5.

**III.C. 2DIR Spectroscopy Measurements of Conformational Dynamics.** 2DIR spectroscopy also monitors the conformational dynamics of the given chemical species by measuring

the time-dependent changes in the diagonal peak lineshapes in the 2DIR spectra.<sup>53,54</sup> While similar information can be extracted from vibrational hole burning measurements,<sup>55,56</sup> Fourier transform 2DIR has the advantage of decoupling the spectral and temporal resolution of the measurement. The impact of spectral diffusion on the 2DIR spectral lineshapes can be understood qualitatively in the following manner. For short times, inhomogeneously broadened diagonal peaks in the 2DIR spectra will be elongated along the surface diagonal, reflecting the strong correlation between the initial  $\omega_\tau$  and the final  $\omega_m$  frequencies. This correlation provides a direct measure of the extent of inhomogeneous broadening for each CN-stretch transition in the 2DIR spectra. As the time delay  $T_W$  increases, the frequency memory decays due to spectral diffusion and the line shape becomes symmetric about the peak center of mass. The center line slope (CLS) method presented by Kwak et al.<sup>54</sup> shows that the normalized frequency–frequency correlation function (FFCF) ( $C(t) = \langle \delta\omega(0)\delta\omega(t) \rangle / \langle \delta\omega(0)\delta\omega(0) \rangle$ ) can be determined from the slope of the signal maximum  $\omega^*$  along the  $\omega_m$  axis as a function of  $\omega_\tau$

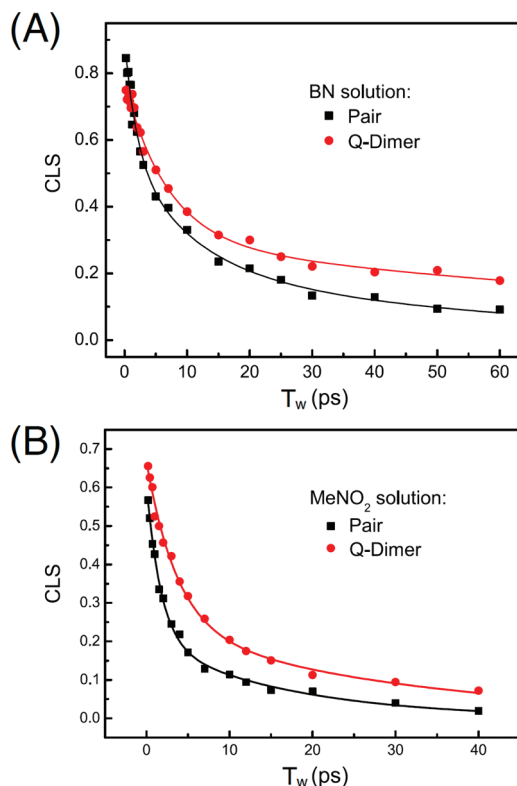
$$C(T_W) \cong C_{\text{CLS}}(T_W) = \frac{\partial\omega^*(\omega_\tau, T_W)}{\partial\omega_\tau} \quad (1)$$

Figure 6 shows  $C_{\text{CLS}}(T_W)$  for the LiNCS ion pair and  $(\text{LiNCS})_2$  Q-dimer in BN and  $\text{MeNO}_2$  solutions. We fit the  $C_{\text{CLS}}(T_W)$  to a biexponential function

$$C_{\text{CLS}}(T_W) = a_1 \exp(-T_W/\tau_1) + a_2 \exp(-T_W/\tau_2) \quad (2)$$

with the fit parameters listed in Table 2. Note that the signal generated by excitation at  $2070 \text{ cm}^{-1}$  may have contributions from the L-dimer structure, as well as the ion pair in  $\text{MeNO}_2$ . For BN, DMC, and EtAct, the L-dimer has a negligible concentration.

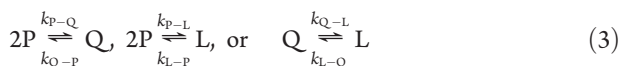
**III.D. Modeling 2DIR Spectra.** We analytically calculated the linear IR spectrum and the  $T_W$ -dependent 2DIR spectra using a



**Figure 6.** Experimental measurement of the inhomogeneously broadened components of the frequency–frequency correlation function (FFCF) for the ion pair and Q-dimer structures in (A) benzonitrile (BN) and (B) nitromethane ( $\text{MeNO}_2$ ) solutions using the center line slope (CLS) method. Note the different time axes for (A) and (B). The parameters extracted from the fit of the experimental data to a biexponential can be found in Table 2.

response function formalism based on diagrammatic perturbation theory with input parameters estimated from the linear and nonlinear experimental results.<sup>41</sup> A detailed description of the two-species exchange kinetic model used in the response function calculation of  $T_w$ -dependent 2D spectra can be found in the work of Kwak et al.<sup>57</sup> As indicated below, the same model can be used to treat the ion pair–dimer system, even for the case of three species chemical exchange applicable to LiNCS dissolved in MeNO<sub>2</sub>.

Here we will present the chemical equations for the Q-dimer (Q), the L-dimer (L), and the ion pair (P)



with  $k_{i-j}$  and  $k_{j-i}$  representing the forward and backward reaction rate constants for the various ionic species. Ignoring the activity coefficients of ionic species in solution, the equilibrium constants equal

$$\begin{aligned} K_{LP} &= \frac{[\text{L}]_{\text{eq}}}{[\text{P}]_{\text{eq}}^2} = \frac{k_{P-L}}{k_{L-P}}, \quad K_{QP} = \frac{[\text{Q}]_{\text{eq}}}{[\text{P}]_{\text{eq}}^2} = \frac{k_{P-Q}}{k_{Q-P}}, \quad \text{or} \\ K_{QL} &= \frac{[\text{Q}]_{\text{eq}}}{[\text{L}]_{\text{eq}}} = \frac{k_{L-Q}}{k_{Q-L}} \end{aligned} \quad (4)$$

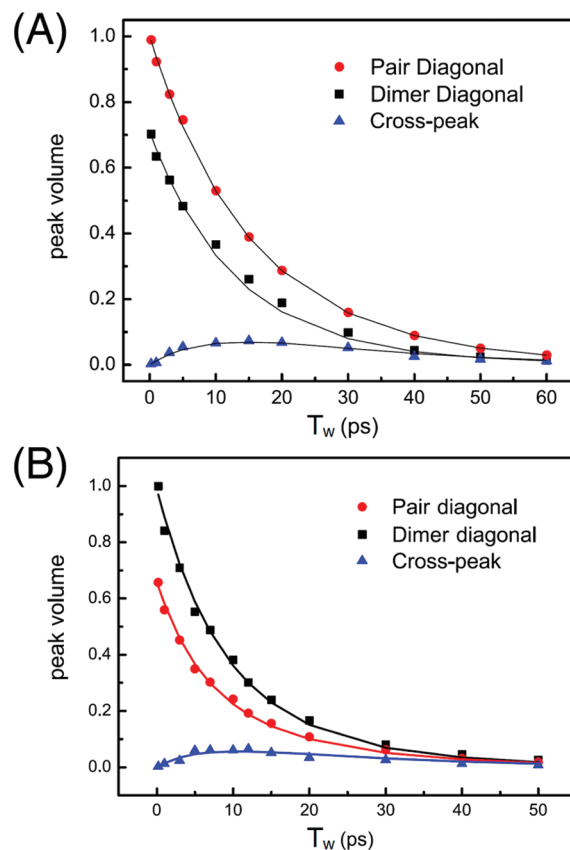


**Figure 7.**  $T_w$ -dependent peak volumes of the ion pair and Q-dimer signals and the cross-peak originating from the Q-dimer dissociation for 1.2 M LiNCS dissolved in (A) benzonitrile and (B) nitromethane. These peak volumes have been extracted from 2D spectra like those shown in Figures 6(A) and 7(A). Note the different time axes for (A) and (B). The chemical exchange time constants extracted from the fit to the experimental data can be found in Table 2.

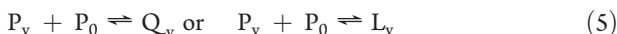
**Table 2. Best Fit Parameters for the FFCF Extracted from the Center Line Slope,  $C(t) = a_1 e^{-t/\tau_1} + a_2 e^{-t/\tau_2}$ , the Relative Concentration of the Ion Pair and Q-Dimer Species, and the LiNCS Ion Pair and Q-Dimer Chemical Exchange Time Constant  $\tau_{\text{ex}}$  in Different Solvents**

solvents	ionic species	$a_1$	$\tau_1$ (ps)	$a_2$	$\tau_2$ (ps)	$\tau_{\text{ex}}$ (ps)	$k_{Q-P}^{-1}$ (ps)
BN	pair	0.5	$3.2 \pm 0.5$	0.38	$40 \pm 5$	$35 \pm 4$	55
	Q-dimer	0.47	$7.0 \pm 1$	0.30	$130 \pm 5$		
$\text{MeNO}_2$	pair	0.37	$1.3 \pm 0.2$	0.18	$18 \pm 3$	$27 \pm 4$	50
	Q-dimer	0.43	$3.6 \pm 0.5$	0.24	$31 \pm 6$		
DMC	pair	0.31	$3.0 \pm 0.4$	0.23	$44 \pm 6$	$36 \pm 5$	56
	Q-dimer	0.38	$4.6 \pm 0.5$	0.25	$81 \pm 10$		
EtAct	pair	0.33	$2.5 \pm 0.2$	0.29	$33 \pm 3$	$35 \pm 7$	42
	Q-dimer	0.28	$2.7 \pm 0.2$	0.32	$57 \pm 5$		

where  $[P]_{\text{eq}}$ ,  $[Q]_{\text{eq}}$ , and  $[L]_{\text{eq}}$  are the equilibrium concentrations of the various ionic species.

The second-order kinetics of the dimerization reactions can be simplified to pseudofirst-order kinetics. We redefine  $[P]_{\text{eq}} = [P]_v + [P]_0$ ,  $[Q]_{\text{eq}} = [Q]_v + [Q]_0$ , and  $[L]_{\text{eq}} = [L]_v + [L]_0$ , with  $[P]_v$ ,

$[Q]_v$  and  $[L]_v$  representing the vibrationally labeled molecules and  $[P]_0$ ,  $[Q]_0$ , and  $[L]_0$  representing the leftover ground-state molecules. Since laser excitation satisfies  $[P]_v \ll [P]_0$ ,  $[Q]_v \ll [Q]_0$ , and  $[L]_v \ll [L]_0$  (we excited  $\sim 5\%$  of the ion pair molecules), the probability of two excited ion pairs combining to form a dimer or the probability of two quanta of vibrational excitation in one dimer is very low. Specifically,  $[P]_v = (J_0\sigma_P)[P]_{eq}$ ,  $[Q]_v = (J_0\sigma_Q)[Q]_{eq}$ , and  $[L]_v = (J_0\sigma_L)[L]_{eq}$ , where  $J_0$  is the photon fluence;  $\sigma_i$  is the absorption cross section of species  $i$ ; and  $J_0\sigma_i$  is the average number of photons absorbed per molecule of species  $i$ .<sup>58</sup> For the low excitation limit,  $J_0\sigma \ll 1$ , we can rewrite the equilibrium equation of the excited molecule subensemble to be



These can be reduced to first-order kinetics with an effective equilibrium constant for the vibrationally excited subensembles equal to  $K_{PQ}^{eff} = \{([Q]_v)/([P]_v)\} = \{(k_{P-Q}^{eff})/(k_{Q-P})\} = \{(\sigma_Q)/(\sigma_P)\} K_{PQ} [P]_{eq}$  and  $K_{PL}^{eff} = \{([L]_v)/([P]_v)\} = \{(k_{P-L}^{eff})/(k_{L-P})\} = \{(\sigma_L)/(\sigma_P)\} K_{PL} [P]_{eq}$  and effective forward reaction rate constants of  $k_{P-Q}^{eff} = \{(\sigma_Q)/(\sigma_P)\} k_{P-Q} [P]_{eq}$  and  $k_{P-L}^{eff} = \{(\sigma_L)/(\sigma_P)\} k_{P-L} [P]_{eq}$ . Since 2DIR spectroscopy only accesses the dynamics of the excited species,  $P_v$  and  $D_v$ , we only directly measure the effective forward reaction rates.

These effective first-order kinetics allow us to use an analytical solution similar to the exchange kinetic model<sup>57</sup> developed by Kwak et al. that accounts for three species exchange. The only complication comes from the fact that the L-dimer has two distinct peaks as discussed above. Thus, we treat the L-dimer as two spectral species when modeling the exchange dynamics. The L-dimer and ion pair equilibrium can be rewritten as



The asterisk marks the vibrationally excited CN stretch, where eq 6 corresponds to excitation of the L-dimer at  $2102 \text{ cm}^{-1}$  and eq 7 corresponds to excitation of the L-dimer at  $2074 \text{ cm}^{-1}$ . For clarity, we label the former as LS-dimer and the latter as LN-dimer. We treat these two excited L-dimers as one chemical species with the same reaction rates and exchange properties, but we view them as two species spectroscopically with different peak positions, population and orientational lifetimes, and FFCFs. We approximate spectral parameters for the L-dimer in eq 7 with those of the ion pair in the response function calculation. The exchange dynamics for excited populations can be described as

$$\begin{aligned} & \frac{d}{dt} \begin{pmatrix} N_{LS}(t) \\ N_{LN}(t) \\ N_P(t) \\ N_Q(t) \end{pmatrix} \\ &= \begin{pmatrix} -k_{L-P} & 0 & k_{P-L}^{eff} & 0 \\ 0 & -k_{L-P} & k_{P-L}^{eff} & 0 \\ k_{L-P} & k_{L-P} & -k_{P-L}^{eff} - k_{P-Q}^{eff} & k_{Q-P} \\ 0 & 0 & k_{P-Q}^{eff} & -k_{Q-P} \end{pmatrix} \begin{pmatrix} N_{LS}(t) \\ N_{LN}(t) \\ N_P(t) \\ N_Q(t) \end{pmatrix} \quad (8) \end{aligned}$$

We have set  $k_{L-Q} = k_{Q-L} = 0$ , consistent with the assumption that the rate of direct exchange between the L-dimer and Q-dimer structures proceeds much more slowly than the rate

of exchange between the dimer structures and the ion pair. This set of linear equations only accounts for the exchange dynamics. Incorporating population and orientational relaxation dynamics is straightforward and has been fully described previously.<sup>28,57</sup> The parameters involved in the calculation are the center frequencies  $\omega_0$ , anharmonicities  $\Delta\omega$ , population lifetimes  $T_1$ , orientation relaxation lifetimes  $\tau_{or}$ , exchange rates, equilibrium concentrations, transition dipole moments  $\mu_{01}$ , and the frequency–frequency correlation functions. The population and orientational relaxation rate have been measured with polarization resolved IR pump–probe measurements, and the results can be found in the Supporting Information. Joint fitting of the FTIR and 2DIR spectrum for  $T_W = 0.2 \text{ ps}$  allows us to fit the transition dipole moments and concentrations for the ion pair and ion-pair dimer since each spectrum depends linearly on the concentration, while the FTIR spectral amplitude is proportional to  $\mu_{01}^2$  and the 2DIR spectral amplitude proportional to  $\mu_{01}^4$ . The frequency–frequency correlation functions influence the vibrational line-shapes in the 2DIR spectra but do not influence the peak volumes. This makes the extraction of chemical exchange dynamics insensitive to the details of the line-shape analysis, particularly when using peak volumes to determine the exchange dynamics.

Figure 7 shows the fit of the experimental peak volumes for the diagonal and cross-peaks for the chemical exchange between the ion pair and the Q-dimer in BN and MeNO<sub>2</sub>. Figures 4(B) and 5(B) show the fit of the 2DIR spectra with the response function calculations. The best fit of the key parameters for the exchange dynamics is shown in Table 2.

## IV. DISCUSSION

Section III has presented the chemical and conformational dynamics of thiocyanate anions in a variety of ionic structures and solvents. We will now discuss these conformational and chemical dynamics and their interdependence.

**IV.A. Spectral Diffusion Dynamics.** The combination of the FTIR absorption spectrum and peak shape analysis of the  $T_W$ -dependent 2DIR spectra provides a detailed measure of the spectral diffusion dynamics as a function of solvent and ionic structure.<sup>53,54</sup> These spectral diffusion dynamics provide a direct measure of the frequency–frequency correlation function (FFCF) and quantify the influence of solvent fluctuations on the CN-stretch frequency of the NCS<sup>−</sup> chromophore. As discussed in Section III.D, we use the center line slope (CLS) method to quantify the FFCFs from the  $T_W$ -dependent 2DIR spectra. The CLS provides an experimental measure of the inhomogeneously broadened contributions to the vibrational line shape but cannot measure the spectral dynamics of motionally narrowed components of the FFCF. Consequently, the plots in Figure 6 do not extrapolate to unity at time zero.

Solvation dynamics reflect the intrinsic dynamics of the solvent weighted by the coupling between those dynamics and the frequency of the optically excited transition utilized in the experiment.<sup>59</sup> Extensive experimental Stark spectroscopy measurements and initial theoretical studies demonstrate that the CN-stretch frequency provides a sensitive measure of local electric fields.<sup>38,39,60,61</sup> We propose that the FFCF measures fluctuations in these electric fields.

The Stark effect leads to changes in the CN-stretch frequency due to transient deviations from the mean value of the local electric field,  $\overrightarrow{\Delta E}$ , as sensed by the change in molecular dipole,  $\overrightarrow{\Delta\mu}_{CN}$ , induced by vibrational excitation of the CN-stretch

vibration

$$\begin{aligned} \hbar \Delta \omega_{\text{CN}} &= - \overrightarrow{\Delta \mu}_{\text{CN}} \cdot \overrightarrow{\Delta E} \\ &= - |\overrightarrow{\Delta \mu}_{\text{CN}}| |\overrightarrow{\Delta E}| \cos \theta \end{aligned} \quad (9)$$

where  $\theta$  represents the angle between  $\overrightarrow{\Delta E}$  and  $\overrightarrow{\Delta \mu}_{\text{CN}}$ . We conclude that electrostatic reorganization dynamics of the solvent directly coordinated to the ion assemblies dominate the observed dynamics for two primary reasons. First, ion pair and Q-dimer structures have very different spectral diffusion dynamics even when dissolved in the same solution. Since the solvent only differs for these distinct ionic structures in close proximity to the ion pair and Q-dimer, these short-ranged distinctions must have a dominant effect on the spectral diffusion dynamics. The sensitivity of vibrational frequencies to short-ranged electric fields has been previously observed for the hydroxyl stretch frequency of water.<sup>62,63</sup> Second, the stronger coordination of BN with  $\text{Li}^+$  than  $\text{MeNO}_2$  and  $\text{Li}^+$  would likely produce slower structural reorganization of the coordinated benzonitrile than the weakly associated  $\text{MeNO}_2$ , consistent with the much slower spectral diffusion dynamics seen for the BN solution.

**IV.B. Chemical Exchange Dynamics.** The solvent dependence of the rate of chemical exchange between the ion pair and Q-dimer has been measured. The rates of chemical equilibration collected in Table 2 show minimal solvent dependence, in contrast with the rates of spectral diffusion, which show pronounced solvent dependence. The contrast is most pronounced when comparing the dynamics in BN and  $\text{MeNO}_2$ . While Q-dimer dissociation into two ion pairs occurs with similar time constants of 50 ps in  $\text{MeNO}_2$  and 55 ps in BN, the slow component of the spectral diffusion dynamics for the Q-dimer has a time constant of 31 ps in  $\text{MeNO}_2$  and 130 ps in BN. Most critically, the rate of Q-dimer dissociation exceeds the rate of spectral diffusion for the Q-dimer in BN, while the reverse occurs for the  $\text{MeNO}_2$  solution. Alternatively, our measurements could indicate that an additional ionic structure exists in the BN solution with a CN stretch absorption spectrum indistinguishable from that of the Q-dimer. We believe this to be a less likely explanation for the observed dynamics for the following reasons. (1) The absorption in the spectral range of the Q-dimer in BN, DMC, and EtAct does not exhibit a broader Gaussian line width than the Q-dimer in  $\text{MeNO}_2$ . On the contrary, the Q-dimer Gaussian width for the  $\text{MeNO}_2$  solution,  $21.2 \text{ cm}^{-1}$ , exceeds that of the three solutions which would hypothetically have the additional ionic species in solution:  $19.5 \text{ cm}^{-1}$  for BN,  $14.3 \text{ cm}^{-1}$  for DMC, and  $14.4 \text{ cm}^{-1}$  for EtAct. (2) We have been unable to identify an additional stable ionic structure in quantum chemical calculations that could be associated with this unresolved ionic structure. (3) Inspection of the CN-stretch of BN shows a spectrally shifted absorption due to solvent coordination of lithium cations that occurs in the LiNCS solution, while inspection of the antisymmetric  $\text{NO}_2$  stretch of  $\text{MeNO}_2$  changes minimally with the dissolution of LiNCS. We do not think the slow spectral diffusion dynamics of the Q-dimer in BN, DMC, and EtAct can be attributed to spectral overlap between the second CN-stretch absorption of the L-dimer with the Q-dimer absorption either since the effect would be largest in the solution with the largest L-dimer concentration, but the Q-dimer in  $\text{MeNO}_2$  solution has the faster conformational dynamics.

We now focus on the mechanistic origin of fast Q-dimer dissociation in the presence of comparatively slow spectral diffusion. As discussed in Section IV.A, we attribute the spectral diffusion dynamics to electric field variations sensed by the CN-stretch frequency. Given the significant variation in the spectral diffusion dynamics measured for the ion pair and Q-dimer in identical solutions, we proposed that the CN-stretch frequency primarily senses electric field fluctuations generated by reorganization of solvent molecules directly coordinated to the  $\text{Li}^+$  cations in the ionic assemblies.

We do not interpret the insensitivity of the Q-dimer dissociation rate to the electrostatic reorganization of the coordinating solvent molecules to be an indication that Q-dimer dissociation does not involve electrostatic reorganization. The reaction must involve significant electrostatic reorganization because the ion pairs produced when the Q-dimer dissociates have large dipole moments, while the reactant Q-dimer has no dipole moment. We have proposed that the slow spectral diffusion results predominantly from electric field fluctuations associated with solvent molecules directly complexed to the  $\text{Li}^+$  cations in the Q-dimer. For both the CN stretch spectral diffusion and the Q-dimer dissociation to be governed in large part by electrostatic reorganization but the slow component of the spectral diffusion to proceed more slowly than chemical dissociation requires the chemical dissociation to be insensitive to the details of the solvent molecules directly coordinated to the  $\text{Li}^+$  cations.

The long-lived Q-dimer spectral heterogeneity strongly indicates that the structural equilibration of  $\text{Li}^+$ -solvent complexes in strongly coordinating solvents occurs more slowly than the association and dissociation of the Q-dimer. While this inversion of the rate of structural equilibration and chemical reaction cannot be accounted for with transition state theory, the impact of the structural heterogeneity on the chemical reactivity has not been determined. If the rate of Q-dimer dissociation depended upon the Q-dimer–solvent conformation, the long-lived conformational heterogeneity of the Q-dimer would lead to heterogeneous dissociation dynamics and generate  $\omega_r$ -dependent rise times for the cross-peaks used to measure the chemical exchange dynamics. While we see no evidence for these heterogeneous dynamics in our 2DIR spectra, the robust characterization of cross-peak lineshapes needed to assess the heterogeneity of the dynamics lies outside our technical capability.

## V. CLOSING REMARKS

Transition state theory assumes the dynamic equilibration of the reactant and product species proceeds much more rapidly than the chemical interconversion of these species. While such a separation of time scales does not occur for photochemical reactions, this separation of time scales for conformational and chemical dynamics has been presumed to generally occur for thermally driven chemical reactions. The presumption need not apply to chemical systems with very slow conformational dynamics or very fast chemical dynamics. While the limit of slow conformational dynamics has been widely investigated in biological systems, the realm of fast chemical dynamics has received minimal attention.

Here we present a time-resolved vibrational spectroscopy study of the interdependence of the conformational and chemical interconversion dynamics of the LiCNS ion pair and the  $(\text{LiNCS})_2$  ion-pair dimer structures. Surprisingly, we have experimentally determined that the rate of ion-pair dimer dissociation

exceeds the rate of ion-pair dimer solvation—the rate of the chemical reaction exceeds the rate of conformational equilibration for the ion-pair dimer. This unusual behavior occurs in solvents that form stable  $\text{Li}^+$ –solvent coordination complexes like benzonitrile but not in a poor Lewis base solvent like nitromethane. We have studied the slow spectral diffusion dynamics of electrostatic reorganization of the solvent molecules directly coordinated to the  $\text{Li}^+$  cations present in the ion-pair dimer structure and concluded that the dissociation of ion-pair dimers depends more critically on longer length scale electrostatic reorganization.

Whether or not these heterogeneous conformational dynamics lead to heterogeneous reaction dynamics has yet to be determined. Heterogeneous reaction dynamics would lead to nonexponential rise times for cross-peaks and inhomogeneous cross-peak lineshapes in the 2DIR spectra. Robustly extracting either experimental signature of heterogeneous reaction dynamics from a 2DIR spectroscopy measurement would be highly challenging and push the present technical limits of 2DIR spectroscopy.

## ■ ASSOCIATED CONTENT

**Supporting Information.** Figures S1–S4 and Tables S1 and S2. This material is available free of charge via the Internet at <http://pubs.acs.org>.

## ■ AUTHOR INFORMATION

### Corresponding Author

\*E-mail: kgaffney@slac.stanford.edu.

### Present Addresses

<sup>†</sup>Department of Chemistry and Chemical Biology, Harvard University, Cambridge, Massachusetts 02138, United States.

## ■ ACKNOWLEDGMENT

This research is supported through the PULSE Institute at SLAC National Accelerator Laboratory by the U.S. Department of Energy, Office of Basic Energy Sciences.

## ■ REFERENCES

- (1) Wigner, E. *Trans. Faraday Soc.* **1938**, *34*, 29.
- (2) Chandler, D. *J. Chem. Phys.* **1978**, *68*, 2959.
- (3) Hanggi, P.; Talkner, P.; Borkovec, M. *Rev. Mod. Phys.* **1990**, *62*, 251.
- (4) Henzler-Wildman, K.; Kern, D. *Nature* **2007**, *450*, 964.
- (5) Hammes-Schiffer, S.; Benkovic, S. J. *Annu. Rev. Biochem.* **2006**, *75*, 519.
- (6) Benkovic, S. J.; Hammes-Schiffer, S. *Science* **2003**, *301*, 1196.
- (7) Garcia-Viloca, M.; Gao, J.; Karplus, M.; Truhlar, D. G. *Science* **2004**, *303*, 186.
- (8) van Oijen, A. M.; Blainey, P. C.; Crampton, D. J.; Richardson, C. C.; Ellenberger, T.; Xie, X. S. *Science* **2003**, *301*, 1235.
- (9) Lu, H. P.; Xun, L. Y.; Xie, X. S. *Science* **1998**, *282*, 1877.
- (10) Kamerlin, S. C. L.; Warshel, A. *Proteins* **2010**, *78*, 1339.
- (11) Olsson, M. H. M.; Parson, W. W.; Warshel, A. *Chem. Rev.* **2006**, *106*, 1737.
- (12) Chabanel, M.; Wang, Z. *J. Phys. Chem.* **1984**, *88*, 1441.
- (13) Chabanel, M.; Lucon, M.; Paoli, D. *J. Phys. Chem.* **1981**, *85*, 1058.
- (14) Goralski, P.; Chabanel, M. *Inorg. Chem.* **1987**, *26*, 2169.
- (15) Vaes, J.; Chabanel, M.; Martin, M. L. *J. Phys. Chem.* **1978**, *82*, 2420.
- (16) Chabanel, M. *Pure Appl. Chem.* **1990**, *62*, 35.
- (17) Baldwin, R. L. *Biophys. J.* **1996**, *71*, 2056.
- (18) Kuhn, T.; Schwalbe, H. *J. Am. Chem. Soc.* **2000**, *122*, 6169.
- (19) Otzen, D. E.; Oliveberg, M. *Proc. Natl. Acad. Sci. U.S.A.* **1999**, *96*, 11746.
- (20) Castleman, A. W.; Holland, P. M.; Keesee, R. G. *J. Chem. Phys.* **1978**, *68*, 1760.
- (21) Hubbard, J.; Onsager, L. *J. Chem. Phys.* **1977**, *67*, 4850.
- (22) Faul, C. F. J.; Antonietti, M. *Adv. Mater.* **2003**, *15*, 673.
- (23) Xu, K. *Chem. Rev.* **2004**, *104*, 4303.
- (24) Moilanen, D. E.; Wong, D.; Rosenfeld, D. E.; Fenn, E. E.; Fayer, M. D. *Proc. Natl. Acad. Sci. U.S.A.* **2009**, *106*, 375.
- (25) Park, S.; Odelius, M.; Gaffney, K. J. *J. Phys. Chem. B* **2009**, *113*, 7825.
- (26) Ji, M. B.; Odelius, M.; Gaffney, K. J. *Science* **2010**, *328*, 1003.
- (27) Gaffney, K. J.; Ji, M. B.; Odelius, M.; Park, S.; Sun, Z. *Chem. Phys. Lett.* **2011**, *504*, 1.
- (28) Ji, M. B.; Gaffney, K. J. *J. Chem. Phys.* **2011**, *134*, 044516.
- (29) Bakker, H. *J. Chem. Rev.* **2008**, *108*, 1456.
- (30) Ji, M. B.; Park, S.; Gaffney, K. J. *J. Phys. Chem. Lett.* **2010**, *1*, 1771.
- (31) Park, S.; Ji, M. B.; Gaffney, K. J. *J. Phys. Chem. B* **2010**, *114*, 6693.
- (32) Baiz, C. R.; Kubarych, K. J. *J. Am. Chem. Soc.* **2010**, *132*, 12784.
- (33) Bian, H. T.; Wen, X. W.; Li, J. B.; Chen, H. L.; Han, S. Z.; Sun, X. Q.; Song, J. A.; Zhuang, W.; Zheng, J. R. *Proc. Natl. Acad. Sci. U.S.A.* **2011**, *108*, 4737.
- (34) Ohta, K.; Tominaga, K. *Chem. Phys. Lett.* **2006**, *429*, 136.
- (35) Dahl, K.; Sando, G. M.; Fox, D. M.; Sutto, T. E.; Owrusky, J. C. *J. Chem. Phys.* **2005**, *123*, 084504.
- (36) Li, M.; Owrusky, J.; Sarisky, M.; Culver, J. P.; Yodh, A.; Hochstrasser, R. M. *J. Chem. Phys.* **1993**, *98*, 5499.
- (37) Lenchenkov, V.; She, C. X.; Lian, T. Q. *J. Phys. Chem. B* **2006**, *110*, 19990.
- (38) Andrews, S. S.; Boxer, S. G. *J. Phys. Chem. A* **2002**, *106*, 469.
- (39) Andrews, S. S.; Boxer, S. G. *J. Phys. Chem. A* **2000**, *104*, 11853.
- (40) Park, S.; Kwak, K.; Fayer, M. D. *Laser Phys. Lett.* **2007**, *4*, 704.
- (41) Khalil, M.; Demirdoven, N.; Tokmakoff, A. *J. Phys. Chem. A* **2003**, *107*, 5258.
- (42) Guerra, C. F.; Snijders, J. G.; te Velde, G.; Baerends, E. J. *Theor. Chem. Acc.* **1998**, *99*, 391.
- (43) Velde, G. T.; Bickelhaupt, F. M.; Baerends, E. J.; Guerra, C. F.; Van Gisbergen, S. J. A.; Snijders, J. G.; Ziegler, T. J. *Comput. Chem.* **2001**, *22*, 931.
- (44) Barthel, J.; Buchner, R.; Wismeth, E. *J. Solution Chem.* **2000**, *29*, 937.
- (45) Paoli, D.; Lucon, M.; Chabanel, M. *Spectrochim. Acta A* **1979**, *35*, 593.
- (46) Schultz, P. W.; Leroi, G. E.; Harrison, J. F. *Mol. Phys.* **1996**, *88*, 217.
- (47) Squalli, O.; Costa, M. C. M.; Cartier, A.; Chabanel, M. *Theochem-J. Mol. Struct.* **1994**, *109*, 11.
- (48) Woutersen, S.; Mu, Y.; Stock, G.; Hamm, P. *Chem. Phys.* **2001**, *266*, 137.
- (49) Zheng, J. R.; Kwak, K.; Asbury, J.; Chen, X.; Piletic, I. R.; Fayer, M. D. *Science* **2005**, *309*, 1338.
- (50) Kim, Y. S.; Hochstrasser, R. M. *Proc. Natl. Acad. Sci. U.S.A.* **2005**, *102*, 11185.
- (51) Golonzka, O.; Khalil, M.; Demirdoven, N.; Tokmakoff, A. *J. Chem. Phys.* **2001**, *115*, 10814.
- (52) Khalil, M.; Demirdoven, N.; Tokmakoff, A. *J. Chem. Phys.* **2004**, *121*, 362.
- (53) Kwak, K.; Park, S.; Finkelstein, I. J.; Fayer, M. D. *J. Chem. Phys.* **2007**, *127*, 124503.
- (54) Kwak, K.; Rosenfeld, D. E.; Fayer, M. D. *J. Chem. Phys.* **2008**, *128*, 204505.
- (55) Gale, G. M.; Gallot, G.; Hache, F.; Lascoux, N.; Bratos, S.; Lecknam, J. C. *Phys. Rev. Lett.* **1999**, *82*, 1068.

- (56) Piletic, I. R.; Gaffney, K. J.; Fayer, M. D. *J. Chem. Phys.* **2003**, *119*, 423.
- (57) Kwak, K.; Zheng, J. R.; Cang, H.; Fayer, M. D. *J. Phys. Chem. B* **2006**, *110*, 19998.
- (58) Ji, M. B.; Park, S.; Connor, S. T.; Mokari, T.; Cui, Y.; Gaffney, K. J. *Nano Lett.* **2009**, *9*, 1217.
- (59) Fleming, G. R.; Cho, M. H. *Annu. Rev. Phys. Chem.* **1996**, *47*, 109.
- (60) Suydam, I. T.; Snow, C. D.; Pande, V. S.; Boxer, S. G. *Science* **2006**, *313*, 200.
- (61) Lindquist, B. A.; Haws, R. T.; Corcelli, S. A. *J. Phys. Chem. B* **2008**, *112*, 13991.
- (62) Smith, J. D.; Saykally, R. J.; Geissler, P. L. *J. Am. Chem. Soc.* **2007**, *129*, 13847.
- (63) Eaves, J. D.; Tokmakoff, A.; Geissler, P. L. *J. Phys. Chem. A* **2005**, *109*, 9424.